JOURNAL OF PROPULSION AND POWER
Vol. 24, No. 5, September–October 2008

Experimental Study of a Dual-Mode Scramjet Isolator

D. B. Le,* C. P. Goyne,† R. H. Krauss,‡ and J. C. McDaniel§
University of Virginia, Charlottesville, Virginia 22904

DOI: 10.2514/1.32591

A constant-area isolator was fabricated and tested in conjunction with a Mach 2 hydrogen–air combustor operating at a simulated Mach 5 flight enthalpy. Predicted isolator performance was validated through pressure measurements obtained via low-frequency pressure taps. The maximum pressure ratio measured in the combustor approached the design limit of 4.5. Scramjet operability, the range of equivalence ratios over which combustion was sustained without shock–inlet interaction, was improved to 0.06–0.32, as opposed to 0.32–0.37 without the isolator. For a given change in fuel equivalence ratio, the location of the shock train was easier to control with the isolator modification. Shock-train location repeatability was found to vary somewhat with equivalence ratio. Small fluctuations in the time-resolved pressure history indicated that the shock train was relatively temporally steady for a given equivalence ratio. High-frequency pressure measurements were within a 95% confidence interval of low-frequency pressure measurements. High-frequency results indicated that an increase in pressure and large pressure fluctuations occurred near the leading edge of the shock train. Power spectral analyses also indicated that there is significant variation in the frequency content of the pressure signal upstream and downstream of the shock-train leading edge. These results suggest that methods of shock-train leading-edge detection may be developed using pressure–time history characteristics other than the pressure magnitude.

Nomenclature

H	=	normal height of the ramp fuel injector
h	=	isolator duct height
L	=	isolator length
M	=	Mach number
n	=	number of samples
P	=	pressure
Re_θ	=	momentum-thickness-based Reynolds number
t	=	time
X	=	scramjet axial location with the origin at the base of the fuel injector
γ	=	ratio of specific heat
θ	=	momentum thickness
σ	=	standard deviation
ϕ	=	equivalence ratio

Subscripts

ref	=	reference quantity at the isolator inlet
1	=	quantity at the isolator inlet
2	=	quantity at the isolator exit and combustor inlet
3	=	quantity at the thermal choke

I. Introduction

INTEREST in single-stage-to-orbit and two-stage-to-orbit vehicles has motivated research and development of ramjet and scramjet engines. Dual-mode scramjets (DMSJ), in particular, are promising propulsion systems for these vehicles because they integrate the advantageous capabilities of both ramjets and scramjets into a single fixed-geometry combustor [1,2]. This combination may enable a vehicle to operate from Mach 3 to Mach numbers approaching 20 with only minor engine geometry changes. At the lower limit of this envelope, the DMSJ operates in ramjet mode and combustion occurs at subsonic speeds. In this mode, the addition of heat can be used to drive the supersonic inflow to sonic conditions and achieve a thermal choke. However, at speeds approaching Mach 7, pressure losses associated with choking the flow increase and operational efficiency decreases [3]. Transition from subsonic to supersonic combustion is obtained by controlling the heat released due to combustion such that the thermal choke is alleviated. Once the heat release is reduced by a sufficient amount, the flow is no longer choked and the flow through the combustor remains largely supersonic [3]. At a given combustor Mach number, the level of heat release may be reduced by reducing the fuel-flow rate. The DMSJ then operates in scramjet mode, in which combustion occurs at supersonic speeds.

If the pressure increase associated with combustion in the DMSJ is high enough, a precombustion shock train is generated and this causes the flow pressure to increase axially from the low pressure at the inlet exit to the high pressure in the combustor. During this mode transition, the shock train manifests itself as a series of oblique or normal shocks upstream of the fuel injector. The shock train is contained between the combustor section and the inlet using an engine section called an isolator. The function of the isolator is to prevent combustor–inlet interaction. However, because the back-pressure increases due to combustion, the shock train must also increase in length so that the low inlet pressure can increase to match the high backpressure boundary condition [3]. The shock train reaches its maximum length following full transition to the subsonic mode. Unstart conditions in the inlet can develop if the shock train reaches the inlet. Unstart conditions are associated with a loss of engine performance, increased drag, decreased mass capture, and lowered engine thrust, which could ultimately result in vehicle loss or mission failure [3]. Thus, it is critical to locate and control the shock train to avoid engine unstart, particularly as the DMSJ operates in, or transitions to, the ramjet mode.

Previous experimental and numerical studies of isolator effectiveness and mode transition have been conducted (e.g., [4–6]). Experimental research conducted by Goyne et al. [6], in particular, investigated transition between supersonic and subsonic combustion in a DMSJ hydrogen–air combustor. Results indicated

Presented as Paper 0023 at the AIAA Aerospace Sciences Meeting and Exhibit, Reno, NV, 10–13 January 2005; received 3 June 2007; accepted for publication 15 December 2007. Copyright © 2008 by the authors. Published by the American Institute of Aeronautics and Astronautics, Inc., with permission. Copies of this paper may be made for personal or internal use, on condition that the copier pay the $10.00 per-copy fee to the Copyright Clearance Center, Inc., 222 Rosewood Drive, Danvers, MA 01923; include the code 0748-4658/08 $10.00 in correspondence with the CCC.

*Graduate Research Assistant, Mechanical and Aerospace Engineering; currently NASA Langley Research Center, Mail Stop 442, Hampton, VA 23602. Member AIAA.

†Research Assistant Professor, Mechanical and Aerospace Engineering, Aerospace Research Laboratory, P.O. Box 400248. Senior Member AIAA.

‡Research Consultant, Rammatek LLC, Aerospace Research Laboratory, P.O. Box 400248.

§Professor, Mechanical and Aerospace Engineering, P.O. Box 400746. Senior Member AIAA.

that dual-mode transition to subsonic combustion was achieved, but that shock–inlet interaction occurred. From these findings, it was determined that an isolator section was necessary to avoid the shock–inlet interaction and to achieve classic DMSJ operation. In the absence of exact theory, the isolator length is typically determined using empirical expressions, such as that due to Billig [1]. Therefore, for the present study, the requirement of a new isolator yields the dual purpose of 1) using the correlation of Billig as a guide for design and then 2) examining the applicability of the correlation through experimental testing: in particular, the applicability in this case to a rectangular scramjet combustor with a single ramp fuel injector. Such a comparison has not been previously made. Further, to develop more advanced prediction tools, the present study presents the opportunity to develop an experimental database for numerical model validation.

In addition to obtaining data for theoretical comparison, installation of a new isolator also enables isolator shock-train studies to be conducted. With the ability to obtain high-frequency pressure–time histories, rather than just time-averaged data, such an experiment can be exploited for scramjet control studies. Only a limited number of studies, such as that by Parrot et al. [7], have examined time-resolved shock-train pressures for an isolator with backpressure imposed via combustion (as opposed to the backpressure of a physical throat). This distinction is deemed important because the combustion process may affect the isolator shock train in a number of ways, not just through the mechanism of a low-frequency backpressure.

Experimental studies by Parrott et al. [7] investigated pressure–time histories in a DMSJ isolator and combustor. The pressure–time histories were sampled at 15.6 kHz with a bandpass filter set in low-pass mode for analysis of frequencies within a 5-kHz bandwidth. The results indicated that the root mean square (rms) pressures ranged from 0.06 to 7.8% of the local dynamic pressure at the boundary-layer edge. Power spectral densities (PSDs) for selected portions of pressure–time histories at different gauge locations were generated and compared. The comparison showed that certain of these PSDs exhibited peaks at certain spectral frequencies. In particular, power spectral densities for pressure–time histories for noncombusting flow, combusting flow, and combusting flow with inlet unstart were all compared. The results showed that the spectral density in each flow type was different. Significant peaks in the power spectral densities for one gage location occurred during flow with combustion. These peaks were described as five tonelike peaks below 1.5 kHz and one broad peak at about 2.4 kHz. Other gage locations did not have the same peaks. The data also showed significant peaks for some gauge locations for the flow with combustion and inlet unstart. The results of this study illustrated that there was a correlation between peaks in the PSD of pressure–time histories and the state of the isolator and scramjet combustor flow. Specifically, the study provided evidence that the peaks were associated with combustion noise propagating upstream. The current study will further explore the relationship between the peaks in the power spectral densities of the pressure–time histories and the location of the shock-train leading edge for the application to shock-train location detection and control.

Measurements of the shock-train location and isolator pressure levels were used previously for DMSJ control purposes in both ground and flight tests. For example, the propulsion system controller of NASA's X-43A (Hyper-X) DMSJ research vehicle monitored isolator pressures to control fuel-flow rates and mitigate the risk of inlet unstart [8]. The successful flight of the X-43A at Mach 7 demonstrated DMSJ and propulsion system controller operation. However, the X-43A tests were not aimed at demonstrating ramjet-scramjet mode transition [8], and no successful flight experiments in mode transition have been reported in the open literature. Thus, studies on the use of isolator pressure measurements to control the DMSJ and the location of the isolator shock train are considered important for future flight test risk reduction. In such control studies, time-resolved measurements of pressure in the isolator are particularly important.

Therefore, in summary, the present investigation seeks to study the isolator flow physics associated with a dual-mode scramjet combustor and to accomplish the following objectives:

1) Design and commission a new DMSJ isolator to enable studies to be conducted of classical dual-mode transition.

2) Assess the performance of the new isolator and the applicability of the correlation due to Billig [1] and evaluate the isolator effects on DMSJ operability.

3) Obtain an experimental database of time-averaged and time-resolved wall pressure that is suitable for analytical and numerical model validation.

4) Investigate time-resolved pressure measurements for potential applicability to a propulsion system controller.

This paper first presents a brief description of the new isolator design and predicted performance. Previous results from direct-connect DMSJ studies by Goyne et al. [6] are first examined. These results are compared with those obtained in the present investigation, in which the new isolator was tested in conjunction with the combustor geometry of Goyne et al. Measured isolator performance and DMSJ operability gains are then examined. Time-resolved measurements of isolator pressure levels are then presented for both steady-state and unsteady combustor equivalence ratios. Pressure–time histories are then finally examined to determine the potential applicability for shock-train location prediction and control in a DMSJ. Specifically, pressure magnitude, standard deviation, and pressure-signal frequency content are examined.

II. Isolator Design

The length of the isolator was designed to achieve a desired maximum pressure ratio between the isolator inlet and exit. As discussed, isolator length is typically determined using empirical expressions, such as those due to Billig [1]. This expression relates the shock-train length L to the isolator pressure ratio P_2/P_1, according to Eq. (1). Isolators are typically constant-area. Thus, the isolator was designed as such, with the isolator height and width fixed to an aspect ratio of 1:1.5 (to match the existing scramjet combustor geometry). From the investigation of Goyne et al. [6], it was found that the maximum pressure ratio measured for the dual-mode scramjet without an isolator was approximately 4.1. Thus, the isolator was designed to achieve a pressure rise of at least this value. In addition, following [3], the maximum achievable pressure rise for an isolator shock train is equivalent to that of a normal shock. From normal shock theory [9], this is equivalent to a pressure ratio of 4.5 for a Mach 2 flow with a specific heat ratio of 1.4. The isolator length was thus determined based on the maximum expected pressure ratio of $P_2/P_1 = 4.5$. The momentum thickness of the DMSJ combustor Mach 2 nozzle was estimated by Goyne et al. [10] from numerical simulations that used an experimentally determined wall temperature of 400 K. The momentum thickness at the isolator's inlet was estimated to be 0.12 mm. Thus, for an inlet Mach number of 2, Eq. (1) predicted the isolator length to be 0.25 m. For the isolator duct height of 25.4×10^{-3} m, this resulted in an L/h of 10.

$$\frac{L(M_1^2 - 1)Re_\theta^{1/4}}{h\sqrt{\theta/h}} = \left[50\left(\frac{P_2}{P_1} - 1\right) + 170\left(\frac{P_2}{P_1} - 1\right)^2\right] \quad (1)$$

As previously discussed, the addition of heat into a supersonic flow causes the Mach number to decrease, and a thermal choke will occur when enough heat is added such that the flow is forced to sonic conditions. To obtain an estimate of the pressure ratio required for a thermal choke to occur in the isolator–combustor configuration, a one-dimensional Rayleigh flow analysis [9] was performed. The combustor area minimally changes, and previous work [6,10] has shown that the fuel–air mixing and combustion is spread out over a large portion of the combustor. Therefore, assuming uniform heat addition for a constant area, and further assuming a calorically perfect gas with a value of 1.4 for the specific heat ratio, the pressure ratio is given by Eq. (2). P_1 and M_1 were previously given, and P_3 and M_3 are the pressure and Mach number, respectively, at the point of the thermal choke. It should be noted that the mixing and

combusting flow downstream of fuel injection actually consists mainly of a mixture of air, hydrogen, and water vapor. However, the ratios of specific heats of these components are relatively close, and given the dependence on Mach number squared, Eq. (2) is regarded as a reasonable approximation. For $M_1 = 2$, the required pressure rise for sonic conditions,$M_3 = 1$, is $P_3/P_1 = 2.8$. Thus, for a one-dimensional flow with a Mach 2 inflow, an isolator may be required for a pressure ratio above 2.8. This result is important for the interpretation of the experimental results presented next, because it will provide an estimate to identify whether the flow is subsonic or supersonic.

$$\frac{P_3}{P_1} = \frac{1 + \gamma M_1^2}{1 + \gamma M_3^2} \tag{2}$$

III. Experiment

A. Facility

The facility used in this study is a vertically mounted, electrically heated, clean-air, continuous-flow type of wind tunnel and is fully described by [10–13]. The facility provides unobstructed physical and optical access to the dual-mode combustor. Compressed air is supplied via an oil-free compressor and desiccant air-dryer system. The air is then heated in a pressurized heater tank via a 300-kW 14-stage electrical resistant heater. Cold air supply enters the top of the heater tank and flows down the outer portion of an annular section. At the lower end of the tank, the air enters the heater core, which houses the resistance heaters. The air flows up through the core to exit from the last heater stage at a temperature approaching 1200 K. The test gas is free of vitiates such as NO, water, particulates, and radical species, unlike vitiated and arc-driven facilities [11–13]. Exiting the electrical resistance heater, the test air flows through a ceramic flow straightener and then passes through a Mach 2 nozzle and the isolator–combustor assembly. The exit of the test section is open to the laboratory, and exhaust gases are removed from the building via an open-ended exhaust tube. A type-K thermocouple probe, which is located in a plenum between the flow straightener and the dual-mode combustor, serves to monitor the facility's stagnation temperature. The stagnation temperature and other operating conditions are listed in Table 1.

B. Combustor

Figure 1 presents a schematic of the dual-mode scramjet geometry. One of the walls, referred to here as the injection wall, locates a single 10-deg unswept compression ramp that is used to introduce fuel into the flow and promote fuel–air mixing. Hydrogen is injected into the flow from the base of the ramp via a conical nozzle that has an exit area ratio equivalent to a Mach 1.7 flow. The centerline of the injection nozzle is parallel to the compression surface of the ramp. All dimensions and distances are normalized by the normal ramp height, $H = 6.35$ mm. The combustor duct-inlet dimensions are $4H \times 6H$, with a 2.9-deg divergence beginning $10H$ downstream of the ramp base on the injection wall. The flow exits the combustor at $58H$ downstream of fuel injection. Pressure-measurement taps are located along the centerline of the combustor on the injection wall, with the exception of two off-centerline pressure taps at $3.88H$ from fuel injection. Combustor wall temperatures are monitored using three type-K thermocouples along the centerline of the injection wall. From

Table 1 Nominal test conditions

Parameter	Air	Fuel
Stagnation pressure, kPa	331	224–1093
Stagnation temperature, K	1010	300
Mach number[a]	2.03	1.7
Static pressure[a], kPa	41	45–221
Static temperature[a], K	600	190
Velocity[a], m/s	977	1781
Equivalence ratio	——	0.06–0.34

[a]Isentropic conditions were calculated at the nozzle exit.

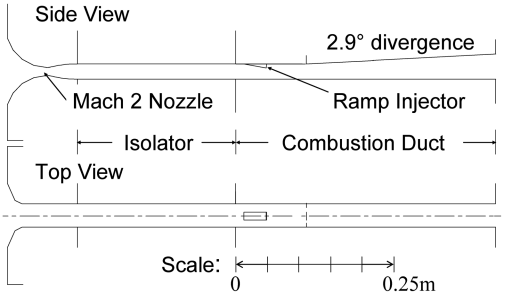

Fig. 1 Schematic of the DMSJ combustor with isolator.

$-8H$ to $26H$ relative to fuel injection, the injection wall and ramp are coated with zirconia to provide thermal protection, and the combustor walls, apart from three optical windows, are water-cooled.

Combustor ignition is achieved via an oxygen–hydrogen wave igniter that feeds hot combustion products into the ramp recirculation region. Further details of the wave igniter can be found in [6,10]. At sufficient ϕ, combustion is self-sustaining after ignition. The lowest value of ϕ for self-sustaining combustion defines the lower bound of scramjet operability in this study.

C. Isolator

The isolator and instrumentation, depicted in Fig. 2, is located between the Mach 2 nozzle and the combustor section. Isolator wall sections are fabricated out of nickel, and all internal isolator flow surfaces are coated with a 0.4-mm-thick layer of zirconia to provide thermal protection. In addition, each of the isolator walls are water-cooled. As already mentioned, the isolator has a constant-area cross section of $4H \times 6H$ and is 10 duct heights long. All instrumentation stations are located along the centerlines of each of the four walls. There are three type-K thermocouples and four low-frequency pressure taps located on each of the four walls. Also, three high-frequency Kulite pressure transducers, model XTEH-10LAC, are on the injection and observation walls (see Fig. 2). The Kulite pressure transducers are recessed-mounted to provide protection from thermal loads. An experimental study was conducted by Adie and Goyne [14] to determine the frequency response of the recessed Kulite pressure transducers to ensure accurate time-resolved measurements. From this study, the response frequency of the mounted transducers was found to be approximately 5 kHz.

D. Data Acquisition

Low-frequency pressure measurements were obtained using a Setra pressure transducer and a Scanivalve® operating at a tap-scanning frequency of 0.5 Hz. A full scan of the combustor and

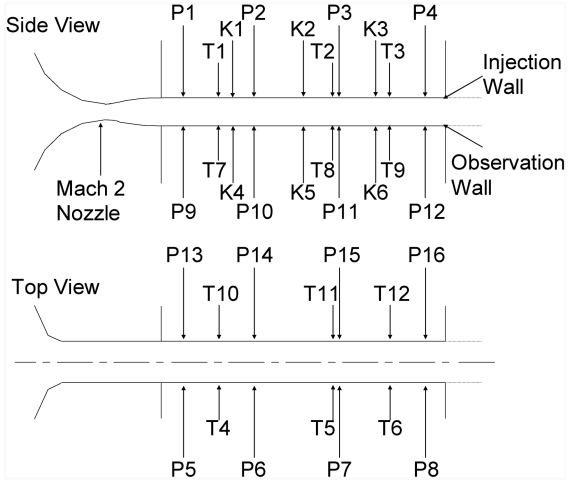

Fig. 2 Schematic of isolator instrumentation locations; K1–K6 are the high-frequency pressure transducers, P1–P16 are the low-frequency pressure taps, and T1–T12 are the type-K thermocouples.

isolator pressure taps was conducted over a period of 60 and 32 s, respectively. Pressure levels, as well as wall temperatures, were recorded using a Fluke Hydra data acquisition unit. High-frequency Kulite pressure signals were acquired using a 12-bit National Instruments NI-6070 data acquisition board. The board was capable of a maximum sampling rate of 1.25 megasamples per second. However, time-resolved pressure measurements were sampled at 10, 25, or 50 kHz.

IV. Results and Discussion

A. Steady-State ϕ

As already stated, the baseline results of Goyne et al. [6] are first examined to determine the effects of the new isolator on the operation of the DMSJ combustor. These results, and those compared next, were obtained for steady-state fuel equivalence ratios. Low-frequency pressure measurements from the study are presented in Fig. 3. The configuration of the combustor is also presented in the figure to provide a physical reference. The test-condition stagnation temperature and pressure were approximately 1160 K and 330 kPa, respectively, and the fuel stagnation temperature was 460 K. All pressures in the figure were normalized by the average nozzle exit pressure for fuel-off, P_{ref}, and are plotted as a function of the normalized distance from the base of the ramp fuel injector. The graph presents the pressure distribution for three fuel conditions: $\phi = 0$, 0.32, and 0.37. The 1-D Rayleigh flow with heat addition analysis value of 2.8 is indicated on the figure to give an estimate of the pressure ratio required for a thermal choke.

For the fuel-off condition, $\phi = 0$, the pressure variations along the combustor indicate the effects of shock and expansion waves generated by the ramp fuel injector. For $\phi = 0.32$, combustion significantly increases the pressure in the combustor. The pressure at the base of the ramp fuel injector is more than three times the pressure measured for the fuel-off condition. However, the pressure on the face of the ramp, at $X = -4.8H$, is equal to that for fuel-off. This indicates that combustion has little or no influence on upstream conditions and that the ramp-induced shock remains attached to the leading edge of the ramp. Thus, the combustor inflow is supersonic and the combustor is operating in scramjet mode. This is consistent with the maximum measured combustor pressure ratio being below the thermal-choke pressure ratio predicted by the 1-D Rayleigh flow analysis. For $\phi = 0.37$, the pressure in the dual-mode scramjet combustor is increased further. The scramjet experiences a pressure rise of more than five times that for fuel-off conditions at the base of the ramp. Downstream of the ramp base at $X = 3.9H$, the combustor experiences a maximum pressure rise of more than four times the average nozzle exit pressure for fuel-off conditions. A rise in pressure over the face of the ramp, as well as upstream, indicates that there is a significant upstream influence due to combustion. The peak pressure level of 4.1 is close to that of a normal shock for Mach 2 flow ($P_2/P_1 = 4.5$), which indicates that the inflow to the combustor is subsonic and that the combustor is operating in the subsonic mode. Shock–inlet, or combustor–nozzle, interaction is evident from the pressure rise measured immediately downstream of the facility nozzle ($X = -7.1H$). Combustion only significantly affects locations upstream of fuel injection when the maximum combustor pressure ratio exceeds the 1-D thermal-choke line. This therefore indicates that Eq. (2) is a reasonable estimate of the point at which a thermal choke occurs. For each of the pressure distributions, the effect of the atmospheric exit condition is evident at the downstream end of the combustor. Finally, it is noted that scramjet operability is limited to between $\phi = 0.32$ and 0.37. Below an equivalence ratio of 0.32, combustion could not be sustained, and above an equivalence ratio of 0.37, shock–inlet interaction occurred.

As previously mentioned, an isolator section was fabricated and tested in conjunction with the DMSJ combustor. The effect of the isolator section on combustor performance and operability can be observed by comparing Figs. 3 and 4. Figure 4 presents typical pressure distributions as a function of axial distance through the modified scramjet for ϕ ranging from 0 to 0.34. A schematic of the isolator–combustor assembly is included in the figure as a reference. All pressures have again been normalized by the nozzle exit pressure. The 1-D Rayleigh flow analysis value is indicated again for reference, as well as the theoretical maximum isolator pressure rise calculated from the empirical relation due to Billig [1].

The pressure distribution for $\phi = 0$ again depicts the shock and expansion waves generated by the ramp fuel injector. As expected, the pressure distribution is similar to the unmodified combustor for this fuel-off condition. The average combustor pressure is higher due to boundary-layer displacement in the isolator. At $\phi = 0.08$, the pressure on the face of the ramp ($X = -4.8H$) is almost equal to that for fuel-off conditions, indicating that combustion has little influence on upstream conditions. The combustor inflow is therefore deemed supersonic and combustion is occurring in the supersonic mode for this equivalence ratio. As the fuel-flow rate is increased, the pressure increase on the ramp face, and upstream, indicates that combustion has an effect on upstream conditions. For each successive increase in ϕ, the pressure on the ramp face also increases. This indicates that the combustor is transitioning from supersonic toward subsonic combustion. For each case, except for $\phi = 0.32$, the maximum measured pressure rise in the combustor is experienced immediately after the ramp base at $X = 3.9H$. For $\phi = 0.32$, the maximum measured pressure rise is on the ramp face ($X = -4.8H$). In addition, combustion influences are experienced further upstream as ϕ is increased, and the shock-train length eventually approaches the length of the isolator at $\phi = 0.32$. However, the lack of pressure rise at the leading pressure tap at $X = -47H$ at this equivalence ratio indicates that the isolator is still able to contain the shock train and isolate the combustor from the facility nozzle. A further increase of ϕ to 0.34, however, was found to cause shock–inlet interaction and force the shock train into the facility nozzle. The maximum pressure rise in the isolator tends toward the predicted theoretical limit of 4.5

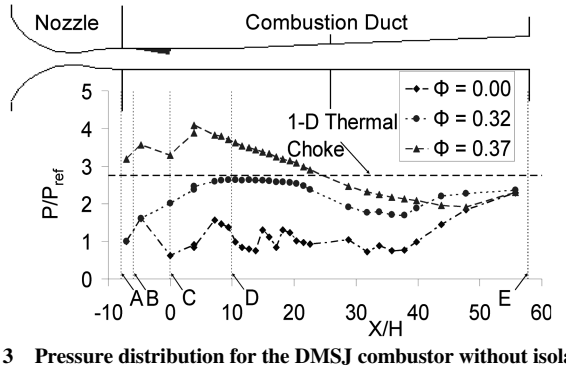

Fig. 3 Pressure distribution for the DMSJ combustor without isolator modification; experimental uncertainty is ±2%, $P_{\text{ref}} = 40$ kPa; the locations are the nozzle exit (A), ramp leading edge (B), ramp base (C), 2.9-deg (divergence begins) (D), and exit (E).

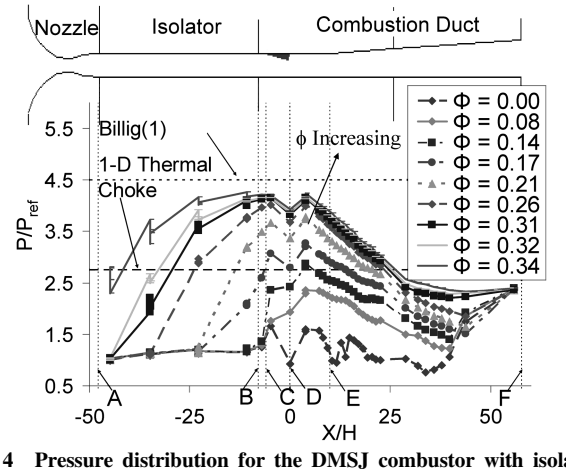

Fig. 4 Pressure distribution for the DMSJ combustor with isolator modification; experimental uncertainty is ±2%, $P_{\text{ref}} = 40$ kPa; the locations are the nozzle exit (A), isolator exit (B), ramp leading edge (C), ramp base (D), 2.9-deg (divergence begins) (E), and exit (F).

as ϕ is increased. At $\phi = 0.32$, the pressure rise at the ramp base is 3.8 times greater than that for fuel-off, and this pressure level is only exceeded on the ramp face with the maximum measured pressure rise of 4.2. The upstream influence of combustion and the magnitude of the pressure rise indicate that the inflow to the combustor is subsonic for this equivalence ratio. The transition from supersonic to subsonic combustion occurs between $\phi = 0.08$ and 0.32. This transition occurs over lower equivalence ratios relative to the configuration with no isolator. This is due to a lower combustor Mach number induced by boundary-layer blockage.

The maximum measured combustor pressure over a range of equivalence ratios is presented in Fig. 5. The data set represents all fueling conditions for which flame holding was achieved but without combustor–nozzle interaction. It can be seen that the maximum pressure rise in the combustor does indeed tend toward the theoretical maximum isolator pressure rise of 4.5. This indicates that the isolator performance is close to that predicted; that is, the isolator length was able to contain the shock train and prevent nozzle interaction up to pressure ratios close to the predicted maximum pressure ratio.

Finally, the effect of the isolator on scramjet operability is assessed from these results. Although the ϕ levels at which both fuel-lean flameout occurs and combustor–nozzle interaction occurs are lower for the combustor with the isolator, as opposed to no isolator, the scramjet operability was improved with the addition of the isolator. The scramjet is able to operate between $\phi = 0.06$ and 0.32 without shock–inlet interaction, as opposed to $\phi = 0.32$ and 0.37 without the isolator. Hence, for a given change in fuel equivalence ratio, the location of the shock train is easier to control with the isolator modification. As may be expected, the addition of the isolator has improved operability of the scramjet combustor.

Repeatability of the isolator operation is now examined. Multiple axial pressure distributions over an equivalence ratio range of $\phi =$ 0–0.27 are presented in Fig. 6 to examine the repeatability of the shock-train location for a given ϕ. Similar shades and line styles indicate equivalent values of ϕ at the nominal test conditions in Table 1. Facility stagnation temperatures and pressures were within 2% of the nominal test conditions. The number of pressure distributions obtained at each ϕ is listed in the legend of Fig. 6. It can be seen in the figure that a high level of shock-train location repeatability was not obtained for all ϕ, which indicates that shock-train location repeatability is sensitive to ϕ. For $\phi = 0.06$ and 0.27, the shock-train location appears to be relatively repeatable. However, at moderate values of ϕ (0.1, 0.17, and 0.21), there is a lower level of shock-train location repeatability. For $\phi = 0.21$, pressures appear to converge downstream of $X = -10H$. These results indicate that the shock-train location in the isolator may vary and may not be consistent for equivalent values of ϕ.

The time-resolved Kulite pressure measurements were used to analyze the shock-train unsteadiness and determine if the lack of repeatability observed was due to pressure fluctuations. These fluctuations are likely induced by the combination of boundary-layer separation and an unsteady backpressure induced through combustion. High-frequency pressure measurements were obtained for a steady ϕ and were averaged over a period of 1 s. The standard deviation was then computed to quantify the fluctuations in pressure. Figure 7 combines low-frequency pressure-tap measurements with the time-resolved, high-frequency pressure measurements. Axial scales are similar to previous figures and the results are grouped according to ϕ. The averaged time-resolved pressures are plotted as data points in the figure, with error bars that depict total error as a 95% confidence interval [15]. The results indicate that the shock train is relatively steady and that the low-frequency measurements are generally within one total error from the mean time-resolved pressure. However, the results do indicate that some of the lack of shock-train repeatability observed may be due to pressure fluctuations in the isolator, as observed in Fig. 6.

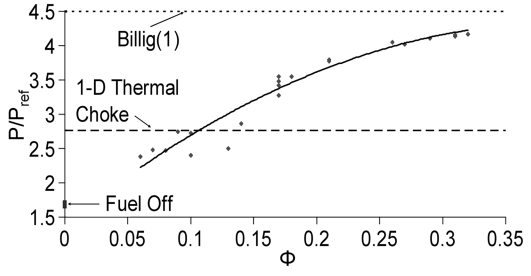

Fig. 5 Maximum measured combustor pressure as a function of equivalence ratio; quadratic curve fit; $P/P_{\text{ref}} = -18.6\phi^2 + 14.8\phi + 1.40$ and $P_{\text{ref}} = 40$ kPa.

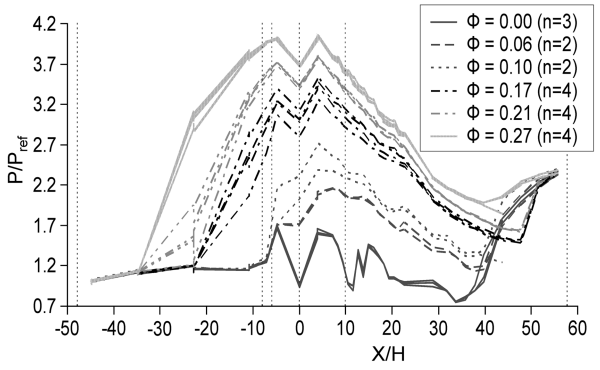

Fig. 6 Repeatability of shock-train location over a range of equivalence ratios; $P_{\text{ref}} = 40$ kPa and n is the number of pressure traces.

B. Unsteady ϕ

Time-resolved pressure measurements for unsteady, or time-varying, fuel equivalence are now examined to assess the applicability to propulsion system controllers. Figure 8 presents an example of the time history of pressure in the isolator as ϕ is increased and then decreased. The corresponding level of ϕ is presented in Fig. 8 as a reference. It can be seen in the figures that as ϕ is increased, a corresponding pressure rise is first measured by the most downstream station of pressure transducers: K3 and K6. This indicates that the increase in combustor pressure pushes the shock train upstream and past the location of the transducers. As ϕ is increased further, corresponding increases in pressure are measured next by K2 and K5 and then by K1 and K4. As ϕ is decreased from its maximum value, the shock train can be seen to be swept back downstream.

These results can be related to those of Fig. 4 and used to interpret the location of the leading edge of the shock train. Referring again to Fig. 8, at low ϕ (less than 0.15), pressure levels are close to the nominal isolator-inlet pressure ($P_{\text{ref}} = 40$ kPa) and are relatively steady. The shock train remains downstream of the isolator and the

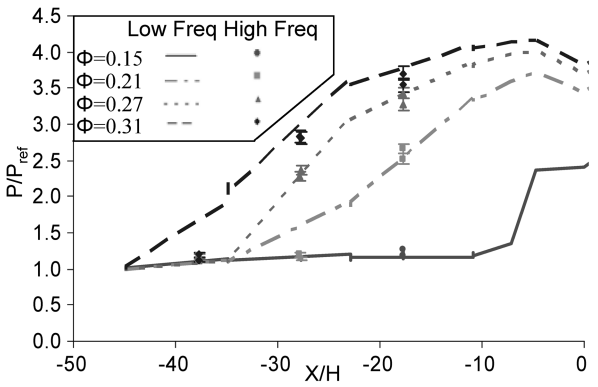

Fig. 7 Comparison of low-frequency wall-pressure distributions with the mean of time-resolved high-frequency wall-pressure measurements for a range of equivalence ratios; error bars represent the total error on the mean; (total error)$^2 = (2\sigma/\sqrt{n}) + (2\%$ experimental uncertainty$)^2$; $P_{\text{ref}} = 40$ kPa

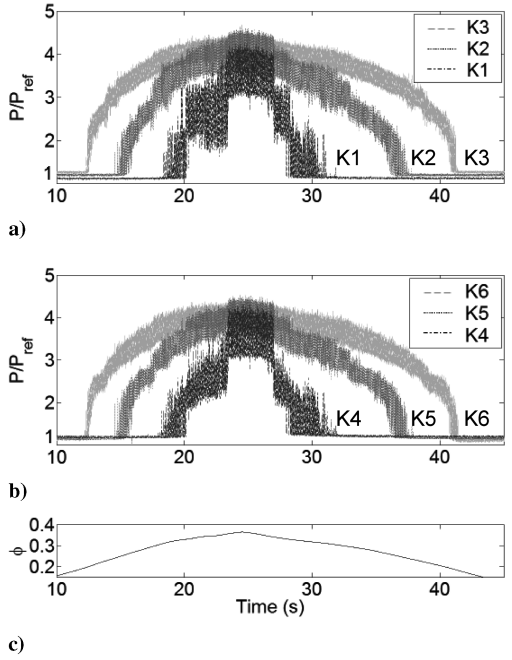

Fig. 8 Typical time-resolved measurements of wall pressure for Kulite transducers a) K1–K3, b) K4–K6, and c) with varying equivalence ratio at a sampling rate of 25 kHz; $P_{\text{ref}} = 40$ kPa.

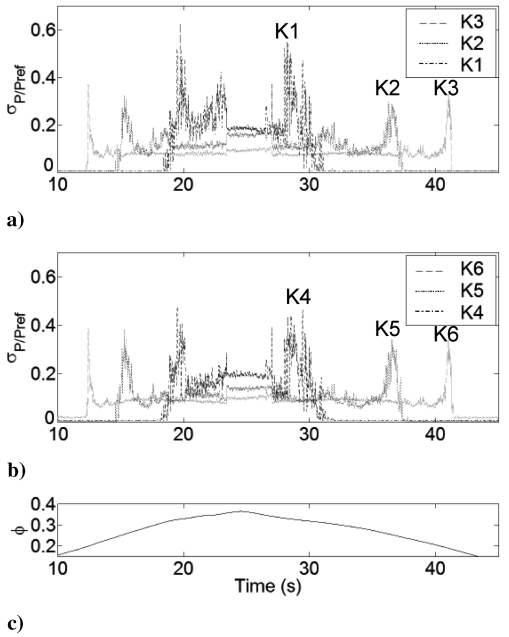

Fig. 9 Standard deviation of time-resolved wall-pressure measurements in Fig. 8 for Kulite transducers a) K1–K3, b) K4–K6, and c) with varying equivalence ratio.

high-frequency transducers. This is consistent with the low-frequency pressure measurements of Fig. 4 for $\phi = 0.08$ and 0.14. However, as ϕ is increased, the pressure measured by K3 and K6 at $X = -17.8H$ increases in magnitude. This indicates that the shock-train leading edge was pushed upstream to this location, and this is again consistent with the results in Fig. 4. A similar result can be observed as ϕ is increased, such that the shock train reaches K2 and K5 at $X = -27.8H$ and reaches K1 and K4 at $X = -37.8H$. Eventually, the shock-train leading edge is upstream of all the Kulite transducers at $\phi = 0.37$. Based on the low-frequency pressure distributions, the shock train is expected to be forced into the facility nozzle above $\phi = 0.32$, and it is interesting to note the corresponding change in time-resolved pressure that occurs from 23 to 27 s in Fig. 8 when ϕ is at this value or above. The effect is particularly evident for K1 and K4, which are the two transducers that are closest to the facility nozzle. This event depicts pressure fluctuations associated with interaction of the combustion induced shock train with the facility nozzle flow.

The time-resolved pressure measurements of Fig. 8 also show variations in the magnitude of pressure fluctuations. These variations were quantified by determining the standard deviation of the measured pressure over a running-time window of 0.05 s. The results are presented in Fig. 9. It is apparent that the standard deviation, or magnitude of the pressure fluctuations, is minimal while the shock train is downstream of each of the high-frequency transducers (at low ϕ). However, as ϕ is increased, there is a marked increase in the standard deviation as the leading edge of the shock train reaches a transducer. As ϕ is increased further, with the leading edge of the shock train pushed past a pressure tap, the standard deviation decreases significantly but is still substantially larger than when the shock is downstream of each location. A similar effect can be observed as ϕ is decreased. It can also be seen that a similar process takes place at each of the transducers, K1 though K6. These results suggest that the standard deviation of the time-resolved pressure may be used to identify the location of the shock train. In particular, the leading edge of the shock train is consistent with a peak in the pressure standard deviation. It is interesting to note that the nozzle interaction event identified in Fig. 8 is also reflected in Fig. 9 as a distinct change in the magnitude of the standard deviation at 23 and 27 s for each of the transducers.

Fourier frequency decomposition was used to decompose the pressure signal, and frequency analysis was completed via a power spectral analysis. As seen in Fig. 8, there exists a significant difference between the pressure signal upstream and downstream of the shock-train leading edge. Via frequency decomposition and power spectral analysis, the frequency content of the pressure signal is now examined over varying values of equivalence ratio. These results investigate the frequency components associated with the pressure signal upstream and downstream of the shock-train leading edge.

As already described, the frequency response of the Kulite pressure tap is approximately 5 kHz. Therefore, the frequency decomposition will examine frequency components only up to 4 kHz. For sampling rates of 25 kHz, this will be equivalent to examining the frequency content over a time window of 0.33 s (8192 samples). Using the pressure signals shown in Fig. 8, the frequency content of the pressure signal upstream and downstream of the shock train at time $t \sim 5$ s ($\phi \sim 0.1$) and $t \sim 19$ s ($\phi \sim 0.32$), respectively, were generated for Kulite pressure transducers K1 and K3 and are shown in Figs. 10 and 11. These figures are a typical representation of the frequency content upstream and downstream of the shock-train leading edge.

Figure 10 indicates that the pressure signal upstream of the shock train is composed of mainly low-power frequency components. The

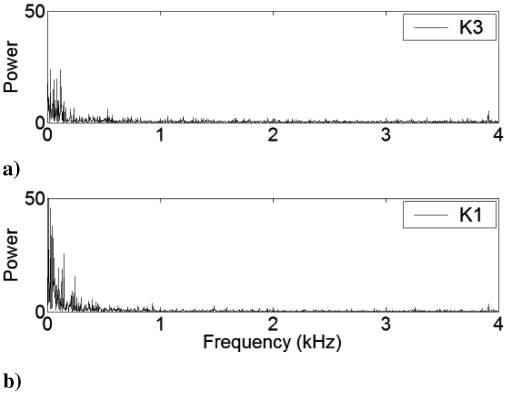

Fig. 10 Typical power spectra for a) K3 and b) K1 for the pressure signal upstream of the shock-train leading edge for the data of Fig. 8 over the time interval $t = 4.9$–5.2 s.

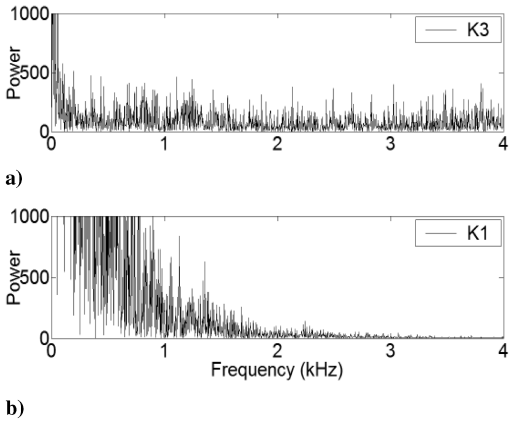

Fig. 11 Typical power spectra generated for a) K3 and b) K1 for the pressure signal downstream of the shock-train leading edge for the data of Fig. 8 over time interval $t = 19.0$–19.3 s.

results from other Kulite pressure transducers show that there are no axial or 2-D variations in the power spectra.

Figure 11 shows typical power spectra for the pressure signal downstream of the shock-train leading edge. These results indicate that the signal downstream of the shock train is composed of a large range of moderate-to-high-power frequency components. This is contrary to the results for the pressure signal upstream of the shock train in Fig. 10. Comparison of the results in Fig. 11 reveals that there is an axial variation of the power spectra in which the power of the frequency components decreases further downstream of the shock-train leading edge. Correlation of these results to the pressure–time history shown in Fig. 8 provides some insight into the relationship that may exist between the location of the shock-train leading edge and the power of the frequency components contained in the pressure signal. The power spectrum in Fig. 11a correlates to the pressure–time history for K3, which is well downstream of the shock-train leading edge. The pressure–time history contains a broad range of frequency components with moderate levels of power. The power spectrum in Fig. 11b correlates to the pressure–time history for K1. At the specified time interval, the shock-train leading edge has a direct influence on pressure transducer, as indicated by the sudden rise in pressure shown in Fig. 8. The power spectrum is characterized by high-power frequency components up to 1 kHz and moderate-power frequency components between 1 and 1.5 kHz.

The results demonstrate that there are distinct differences in the spectral characteristics of the pressure signal and that these differences are due to the relative location of the pressure transducer to the leading edge of the shock train. The pressure–time histories in Fig. 8 indicate that at time 19.0 to 19.9 s, the K1 transducer is located immediately downstream of the shock-train leading edge and the K3 transducer is located far downstream of the leading edge. Thus, inspection of Fig. 11 reveals that the boundary-layer separation induced by the shock-train leading edge has a distinct spectral characteristic that is different from the undisturbed boundary layer and from that well downstream of the shock-train leading edge. Although no one dominant frequency was evident downstream of the shock-train leading edge, the results suggest that as the separated region grows and develops downstream of the shock-train leading edge, due to downstream shock-train/boundary-layer interactions, the spectral characteristics change and the spectra of the wall pressure reflects a profile with a power that is more spread out over the spectrum.

These results indicate that there is a significant difference in the frequency content of the pressure signal upstream and downstream of the shock train. Upstream of the shock train, the content of the pressure signal is largely dc. Downstream of the shock train, the pressure signal is composed of high-power, low- and high-frequency content that changes relative to the shock-train leading-edge location.

In summary, the shock-train leading edge therefore causes a significant change in the magnitude, standard deviation, and spectral characteristics of the time-resolved pressure in the isolator. Each of these three quantities are thus candidates for use by a propulsion system controller as part of a feedback control system of a scramjet. Such a system could be used to prevent events such as isolator–inlet interaction if the location of the leading edge of the shock train can be accurately determined and controlled. Pressure magnitude has traditionally been considered to be a candidate for such feedback control. However, these results show that standard deviation, or rms information, and spectral characteristics of the time-resolved pressure could also be used. This finding has not been previously reported and is regarded as significant because these pressure-signal characteristics could be used as additional inputs to a controller, and this could be used to improve the accuracy and robustness of the control system.

V. Conclusions

This investigation presented a study on the isolator flow physics of a dual-mode scramjet. Test conditions simulated Mach 5 enthalpy and experiments were conducted using a new isolator in direct-connect tests. A 10-duct-height-long isolator was fabricated and integrated with an existing combustor, and low-frequency and time-resolved pressure measurements were obtained throughout the isolator–combustor configuration for a range of fuel equivalence ratios. The performance of the new isolator was close to the empirical correlations of Billig [1], and pure subsonic combustion resulted in a shock train that did not reach the facility nozzle. The addition of the isolator improved scramjet operability, increasing the operational fuel equivalence range from 0.32–0.37 to 0.06–0.32, and the DMSJ was able to operate through the classical mode-transition regime. Shock-train location repeatability was found to vary somewhat with ϕ. High- and low-frequency pressure measurements were combined to analyze shock-train unsteadiness and repeatability. It was found that the shock train was relatively stable with time-resolved pressure fluctuations generally within a 95% confidence interval of the low-frequency pressure. High-frequency pressure measurements exhibited a variation in pressure fluctuation intensity relative to the leading edge of the shock train. The pressure fluctuations were quantified by computed standard deviation, which showed a maximum value near the leading edge of the shock train.

Preliminary spectral analyses also identified characteristic differences between the frequency content of the pressure signal upstream and downstream of the shock-train leading edge. Although no one dominant frequency was evident downstream of the shock-train leading edge, the results suggest that shock-train location can be identified from quantities other than the magnitude of the measured pressure. Evidence was found that these quantities can be used to predict the onset of the leading edge of the shock train. Although further research is necessary, the results indicate that algorithms using time-resolved isolator pressure measurements can be used to enhance control of a DMSJ combustor during mode transition. It is anticipated that further study of the generated database will lead to a better understanding of the isolator flow physics and this will accelerate the development of new control strategies. In particular, the database is now available for numerical model validation and this activity will further enable a deeper understanding of the flow and its control.

Acknowledgments

The authors appreciate the financial support of the National Institute of Aerospace (NIA) under NIA project 3002-VA with A. H. Auslender of NASA Langley Research Center as technical monitor. Testing was also supported by NASA under grant NAG-1-02019 with C. R. McClinton and D. E. Reubush of NASA Langley Research Center as technical monitors. Discussions with K. E. Rock of NASA Langley Research Center are also appreciated. The authors also appreciate the contribution of P.F. Adie in isolator engineering design and the contribution of C. G. Rodriguez of Alliant Techsystems Inc., General Applied Science Laboratory (ATK-GASL) in performing the referenced numerical simulation.

References

[1] Billig, F. S., "Research on Supersonic Combustion," *Journal of Propulsion and Power*, Vol. 9, No. 4, 1993, pp. 499–514.

[2] Cockrell, C. E., Jr., Auslender, A. H., Guy, R. W., McClinton, C. R., and Welch, S. S., "Technology Roadmap for Dual-Mode Scramjet Propulsion to Support Space-Access Vision Vehicle Development," AIAA Paper 2002-5188, 2002.

[3] Heiser, W. H., and Pratt, D. T., *Hypersonic Airbreathing Propulsion*, AIAA Education Series, AIAA, Washington, D.C., 1994.

[4] Sullins, G. A., "Demonstration of Dual Mode Transition in a Scramjet Combustor," *Journal of Propulsion and Power*, Vol. 9, No. 4, 1993, pp. 515–520.

[5] Reinartz, B. U., Herrmann, C. D., and Ballmann, J., "Aerodynamic Performance Analysis of a Hypersonic Inlet Isolator Using Computation and Experiment," *Journal of Propulsion and Power*, Vol. 19, No. 5, 2003, pp. 868–875.

[6] Goyne, C. P., McDaniel, J. C., Quagliaroli, T. M., Krauss, R. H., and Day, S. W., "Dual-Mode Combustion of Hydrogen in a Mach 5, Continuous-Flow Facility," *Journal of Propulsion and Power*, Vol. 17, No. 6, 2001, pp. 1313–1318.

[7] Parrott, T. L., Jones, M. G., and Thurlow, E. M., "Unsteady Pressure Loads in a Generic High-Speed Engine Model," NASA TP 3189, 1992.

[8] Jones, P. T., and Baumann, E., "Evaluation of the X-43A Scramjet Engine Controller Performance by Monte Carlo Technique," AIAA Paper 2003-5192, 2003.

[9] Anderson, J. D., Jr., *Modern Compressible Flow with Historical Perspective*, McGraw–Hill, Boston, 1990.

[10] Goyne, C. P., Rodriguez, C. G., Krauss, R. H., McDaniel, J. C., and McClinton, C. R., "Experimental and Numerical Study of a Dual-Mode Scramjet Combustor," *Journal of Propulsion and Power*, Vol. 22, No. 3, 2006, pp. 481–489.

[11] Krauss, R. H., and McDaniel, J. C., "A Clean Air Continuous Flow Propulsion Facility," AIAA Paper 92-3912, 1988.

[12] Krauss, R. H., McDaniel, J. C., Jr., Scott, J. E., Jr., Whitehurst, R. B., III, Sega, C., Mahoney, G. T., and Childers, J. M., "Unique, Clean-Air, Continuous-Flow, High-Stagnation-Temperature Facility for Supersonic Combustion Research," AIAA Paper 88-3059, 1988.

[13] Goyne, C. P., McDaniel, J. C., Krauss, R. H., and Whitehurst, W. B., "Test Gas Vitiation Effects in a Dual-Mode Scramjet Combustor," *Journal of Propulsion and Power*, Vol. 23, No. 3, 2007, pp. 559–565. doi:10.2514/1.24663

[14] Adie, P. F., and Goyne, C. P., "An Investigation of Pressure Tap Geometries and Their Relationship to Transducer Rise Time," B.S. Thesis, Univ. of Virginia, Charlottesville, VA, 2004.

[15] Coleman, H. W. and Steele, W. G., "Engineering Application of Experimental Uncertainty Analysis," *AIAA Journal*, Vol. 33, No. 10, 1995, pp. 1888–1896.

L. Maurice
Associate Editor